We are IntechOpen,
the world's leading publisher of
Open Access books
Built by scientists, for scientists

6,900
Open access books available

185,000
International authors and editors

200M
Downloads

154
Countries delivered to

Our authors are among the

TOP 1%
most cited scientists

12.2%
Contributors from top 500 universities

BOOK CITATION INDEX
CLARIVATE ANALYTICS
INDEXED

WEB OF SCIENCE™

Selection of our books indexed in the Book Citation Index
in Web of Science™ Core Collection (BKCI)

Interested in publishing with us?
Contact book.department@intechopen.com

Numbers displayed above are based on latest data collected.
For more information visit www.intechopen.com

Fabrication and Characterization of Nanoscale Shape Memory Alloy MEMS Actuators

Cory R. Knick

Abstract

The miniaturization of engineering devices has created interest in new actuation methods capable of large displacements and high frequency responses. Shape memory alloy (SMA) thin films have exhibited one of the highest power densities of any material used in these actuation schemes and can thermally recovery strains of up to 10%. Homogenous SMA films can experience reversible shape memory effect, but without some sort of physical biasing mechanism, the effect is only one-way. SMA films mated in a multi-layer stack have the appealing feature of an intrinsic two-way shape memory effect (SME). In this work, we developed a near-equiatomic NiTi magnetron co-sputtering process and characterized shape memory effects. We mated these SMA films in several "bimorph" configurations to induce out of plane curvature in the low-temperature Martensite phase. We quantify the curvature radius vs. temperature on MEMS device structures to elucidate a relationship between residual stress, recovery stress, radius of curvature, and degree of unfolding. We fabricated and tested laser-irradiated and joule heated SMA MEMS actuators to enable rapid actuation of NiTi MEMS devices, demonstrating some of the lowest powers (5–15 mW) and operating frequencies (1–3 kHz) ever reported for SMA or other thermal actuators.

Keywords: MEMS, phase-change, shape memory alloy, microactuators, optical actuation, electrical actuation, microrobotics, smart materials, nanoscale

1. Introduction

One of the earliest reported thin film version of Nickel-Titanium shape memory alloy was done in 1990 [1]. The first several accounts of SMA film characterization on Si wafers showed measureable shape memory effects, but all transformations happened below ambient conditions, in part due to the fact that the films tended to be Ni-rich in composition if starting from equiatomic NiTi sputter target, due to the different sputter yields of Ni and Ti. Ni has a higher sputter rate than Ti, and Ti has a tendency to react with any residual oxygen in the deposition chamber. In order to make high performance thermal actuators, it is thus necessary to undergo the necessary processing to ensure transformations are measured above ambient conditions [2]. This is no easy task, but can nonetheless be done by carefully controlling Ni/Ti ratio and thermal processing (i.e., annealing). One of the first SMA-based MEMS actuators was reported out of Case Western University (CWU) in 2001, based on a

sputtered NiTi film capable of recovering about 250 MPa according to their stress-temperature loop on 4" Si wafer [2].

Of the many SMAs available, NiTi has become one of the most widely used due to its exceptional physical and mechanical properties (SME and SE), including large recoverable strains [3]. To understand the reason behind the SME/SE in NiTi, it is necessary to first understand the crystallography. The basis for SME/SE is the switching between two different crystallographic phases, namely the high temperature phase known as austenite (or) the parent phase, and the low temperature phase known as Martensite. The crystal structure of the austenite phase is a CsCl type B2 cubic structure and the low temperature Martensite phase is a complex monoclinic crystal structure (B19'). The martensitic transformation is a diffusionless solid-state phase transformation. During the martensitic transformation, the metal atoms move cooperatively in the matrix under shear stresses. As a result a new phase is formed from the parent phase. To accommodate the internal stresses caused by the transformation to the B19' phase, the formation of a combination of up to 24 multiple martensitic variants is possible, resulting in a twinned Martensite crystal form, also known as self-accommodated Martensite.

TiNi thin films are in demand for applications in actuators for micro-electromechanical systems (MEMS) [4–12], because these films exhibit large displacement, accompanied by the shape memory effect (SME) through the B2 austenite to B19' monoclinic Martensite transformation. The majority of TiNi films are fabricated by RF or DC magnetron sputtering methods [13–20], and these films are amorphous, unless the substrates are heated during deposition [16, 20]. Post deposition annealing at a temperature above 700 K (equivalent to 427°C) for crystallization is necessary for the films initially deposited in amorphous condition to show the shape memory effect [21]. It is noted that Ti–Ni thin films sputter-deposited at ambient temperature are often amorphous, thus require post-sputtering crystallizing at elevated temperature to obtain the desired shape memory property. It is also possible to crystallize TiNi films during deposition by utilizing a heated substrate above an ambient temperature [22]. The TiNi films deposited in this manner exhibit interesting behaviors such as lowered crystallization temperature and oriented crystallographic structure [18, 19]. For example, Ikuda observed that the NiTi film deposited onto a glass substrate at 673 K (or 400°C) produced crystallinity in the NiTi film. Other, more recent studies also looked into the SMA properties of in-situ annealed NiTi films.

Regarding the in-situ crystallization of NiTi, Gisser also observed that the films deposited on (100) silicon (Si) substrates at 733 K (equivalent to 500°C) showed a (110)-oriented crystalline structure of the austenite phase [23]. By incorporation of a Ru seed layer, epitaxial growth of the NiTi alloy can be achieved at some of the lowest deposition and crystallization temperatures, and thinnest films reported to date [24]. Hou also observed that the films deposited onto quartz and polyimide substrates above 623 K (equivalent to 350°C) showed a strong (110)-oriented crystalline structure [25–28]. This range of crystallization temperatures of the TiNi films suggests that the crystallization process is affected by the surface condition of the substrates. However, it is not clear why the heated substrates lowers the crystallization temperature and enhances a particular orientation for the TiNi thin films. This is due to lack of understanding the process of film growth during deposition. The composition and structure of sputtered Ni-Ti shape memory alloy (SMA) films are significantly affected by the sputtering conditions: target power, gas pressure, target to substrate distance, deposition temperature, substrate bias voltage, etc.

Some fundamental limitations for shape memory MEMS are related to (1) how thin could one go and still be able to measure reversible shape memory effects,

(2) how fast could one conceivably actuate the SMA MEMS device (limitations previously existed) that would not allow for heat transfer to happen much faster than several 10s, or at most, 100 Hz. Several accounts claim that NiTi films should be at least 100–400 nm thick [15] to help ensure shape memory effects which can be suppressed by film/substrate interfacial strains and small grain sizes [29–33].

Combined with SMA's natural advantages of large displacements, and high work densities [8], our efforts have demonstrated major breakthroughs in the bandwidth, or speed with which NiTi could be actuated, and thus enabled additional possibilities to use NiTi in microelectronics and MEMS. Shape memory MEMS can certainly now be used for higher frequency actuation applications such as mechanical logic, signal routing, and switching, and at relatively low power and energy consumption. In thin films the roll of texture is extremely important in improving shape memory properties like reversible strain [34].

In the preceding paragraphs we overviewed the important developments in NiTi thin films processing and characterization. As such, we aim to use the next paragraph to highlight some of the more relevant MEMS device implementations of NiTi SMA films.

In 2004, high frequency actuation based on SMA MEMS was only 20–40 Hz [35], and considerable improvements have been made since then. By shrinking the volume and heat capacity of the SMA MEMS actuators, we showed for the first time, reversible actuation beyond 1 kHz frequencies, verifying that the heat transfer (in other words, the heating and cooling of shape memory alloy), could happen more than 1000 times per second. For example, green laser actuation of shape memory MEMS bimorph actuators was characterized in [9], whereby actuation response happened in just a few milliseconds. Here, the authors showed that NiTi bimorph cantilevers with nanometer thickness NiTi, could be actuated in under 100 ms, with as little as 2 W/cm^2. In another paper, the high cycle frequency of actuation and electrical characterization of SMA MEMS device was characterized to include (resistance, current, and power requirements) [5]. Here, it was demonstrated that NiTi bimorph resistor actuators could be actuated with as little as 0.5 V, requiring just 5–15 mA of power, and at rates faster than 1000 times per second (up to 3 kHz) due to the small volume and rapid heat transfer facilitated by large surface to volume ratios. Expanding upon this work even further, these same NiTi films were integrated with nanoscale 3D printing to enable some impressive actuation metrics [36, 37]. Specifically, by 3D printing polymeric materials mated with NiTi films, the following metrics were achieved: >5000 reversible actuation cycles with very limited degradation, low voltage actuation of 3.7 V (which is compatible with common Li-ion batteries), large strokes (85 µm for 415 µm length cantilever), and large force-displacement product of 1.2×10^{-7} N-m, with an impressively small volume and weight (1.04×10^{-5} cm^3 and 1.27×10^{-5} g, respectively). By comparison in [38], 1.6 kHz actuation frequency was achieved using a pulsed laser to actuate a FIB cut NiTi SMA microactuator spring of 25 µm thickness. Most recently NiTi SMA has even recently been integrated with Si photonics to form a physically actuated optical coupler/de-coupler type device with excellent nano-positioning accuracy to within 4 nm and on/off ratio of 9 dB [7, 39].

2. Methods

2.1 Stress vs. temperature measurements

Stress versus temperature measurements were performed using a Toho FLX-2320-S wafer bow tool with controlled heating and cooling from 25 to 100°C with a heating

and cooling rate of 1°C/min. For these experiments, we prepared films of NiTi by sputtering onto 4-inch silicon (Si) wafers and vacuum annealing at 600, 500, and 450°C to crystallize the material. Additionally, we measured several NiTi on Si wafers where the NiTi was sputtered under 600°C substrate conditions. In later efforts, we characterized these films with NiTi in-situ anneals of 325, 350, 375, 400, 425, and 500°C. Wafer bow was measured experimentally from 25 to 100°C at a 1°C/min heating and cooling rates, which allowed us to calculate and plot the temperature-dependent residual stress in the NiTi film for each wafer sample based on Stoney's equation (1).

$$\sigma = \frac{E}{6(1-\nu)}\frac{h_s^2}{h}\left(\frac{1}{R} - \frac{1}{R_o}\right) \tag{1}$$

Here, σ is the stress in the thin film, and E, ν, and h_s are Young's modulus of Si, Poisson ratio of the Si substrate and the thickness of the Si substrate, respectively. h represents the NiTi thin film thickness and R and R_o represent the radii of curvature of the NiTi film- Si substrate composite and the curvature of the bare Si substrate. We used an extended version of Stoney's equation (2) in order to calculate the stress in the NiTi layer when deposited on a thin Pt film on Si wafer. Here, σ_{NiTi} is the stress in the NiTi layer, and σ_{Pt} represents the stress in the annealed Pt layer. The variable h_{NiTi} represents the NiTi thin film thickness, and R and R_o represent the radii of curvature of the NiTi film and the annealed Pt/Si substrate, respectively.

$$\sigma_{NiTi} = \frac{E\,h_s^2}{6(1-\nu)\,h_{NiTi}}\left(\frac{1}{R} - \frac{1}{R_o}\right) - \left(\frac{6(1-\nu)}{E}\right)\left(\frac{\sigma_{Pt}(h_{NiTi+Pt} - h_{NiTi})}{h_s^2}\right) \tag{2}$$

2.2 Laser actuation of SMA MEMS

We also used a 400 mW, 532 nm green laser exiting a 400 μm diameter optical fiber to irradiate and heat released cantilevers with a known optical intensity level. We used optical density filters (ThorLabs) to control the laser irradiance levels. The distance from the optical fiber exit and therefore laser spot size were fixed at 1 mm, which allowed calculation of the optical intensity. We used a Photron Fastcam camera connected to a microscope to record video at 2000 frames per second (fps) or more to measure temporal data on activation time.

2.3 Electrical actuation (joule heating) SMA MEMS

We build stressed bimorph actuators out of SU-8 and NiTi, whereby a pulsed current through the freestanding NiTi 'resistor' caused rapid heating and cooling through Joule Heating. Deflection was monitored using laser Doppler Vibrometry (LDV) experimental setup. A Keithly power meter was used to pulse current (square wave) at various frequencies (2–3000 Hz) through the NiTi resistively heated MEMS actuator.

3. Results and discussion

3.1 Stress vs. temperature measurements

Figure 1A shows a reversible phase change with onset at 60°C upon heating for two different NiTi sputter deposition pressures of $Ni_{50}Ti_{50}$ on 200 nm Pt. Since NiTi was sputtered onto a thin film of Pt on Si for this set, the modified Stoney's equation (2) was used to figure the NiTi film stress. Assuming the thickness of the two films to be similar, the film sputtered at 5 mTorr exhibited a higher value of recovery stress,
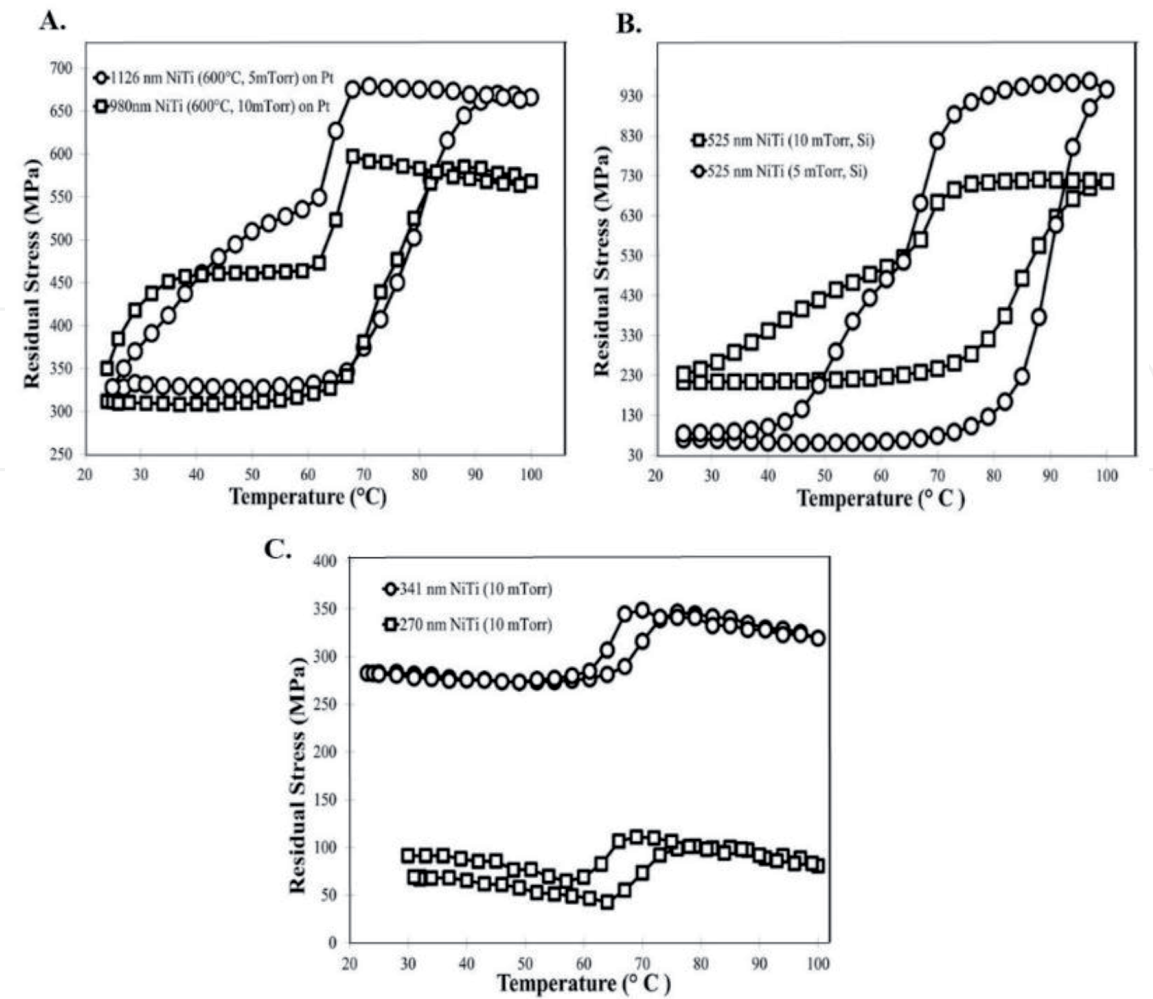
Figure 1.
(A) Stress vs. temperature plots for NiTi sputtered at 600°C under different pressures onto 200 nm Pt for NiTi (A) near 1 μm thickness, (B) near half micron thickness, and (C) approaching 200 nm minimum film thickness for SMA properties.

defined as the difference between initial stress and stress in the presumably austenitic phase at elevated temperature. Both films had a similar initial or residual stress of around 300 MPa. The maximum residual stress values peaked around 70°C for each wafer in this experiment, and the process was reversible when cooled back to RT.

Figure 1B shows that the trend of higher recovery stress (approximately 900 MPa) at lower deposition pressure was the same for two 525 μm thick NiTi films, which in this case were deposited onto Si and stress values were determined with standard Stoney equation (1). Residual stress was lower (70 MPa) for NiTi sputtered onto Si at 5 mTorr compared to the NiTi sputtered at 10 mTorr (230 MPa). Lower residual stress would generally be desired to reduce unwanted deformation of MEMS structures fabricated based on NiTi. These results are also useful, providing confirmation that the SME is similar when we deposited NiTi onto Pt or Si.

We also performed wafer bow stress measurements on thinner films of 341 and 270 nm NiTi which were sputtered onto Si at 600°C substrate temperature. **Figure 1C** shows a reversible SME in 341 and 270 nm films sputtered at 10 mTorr. Therefore, significant micro actuation should be achievable in even thinner films.

3.2 Laser actuation of SMA MEMS

We measured cantilever actuation under optical irradiation. Devices demonstrated rapid actuation ranging from 2 to 90 ms, depending on optical power
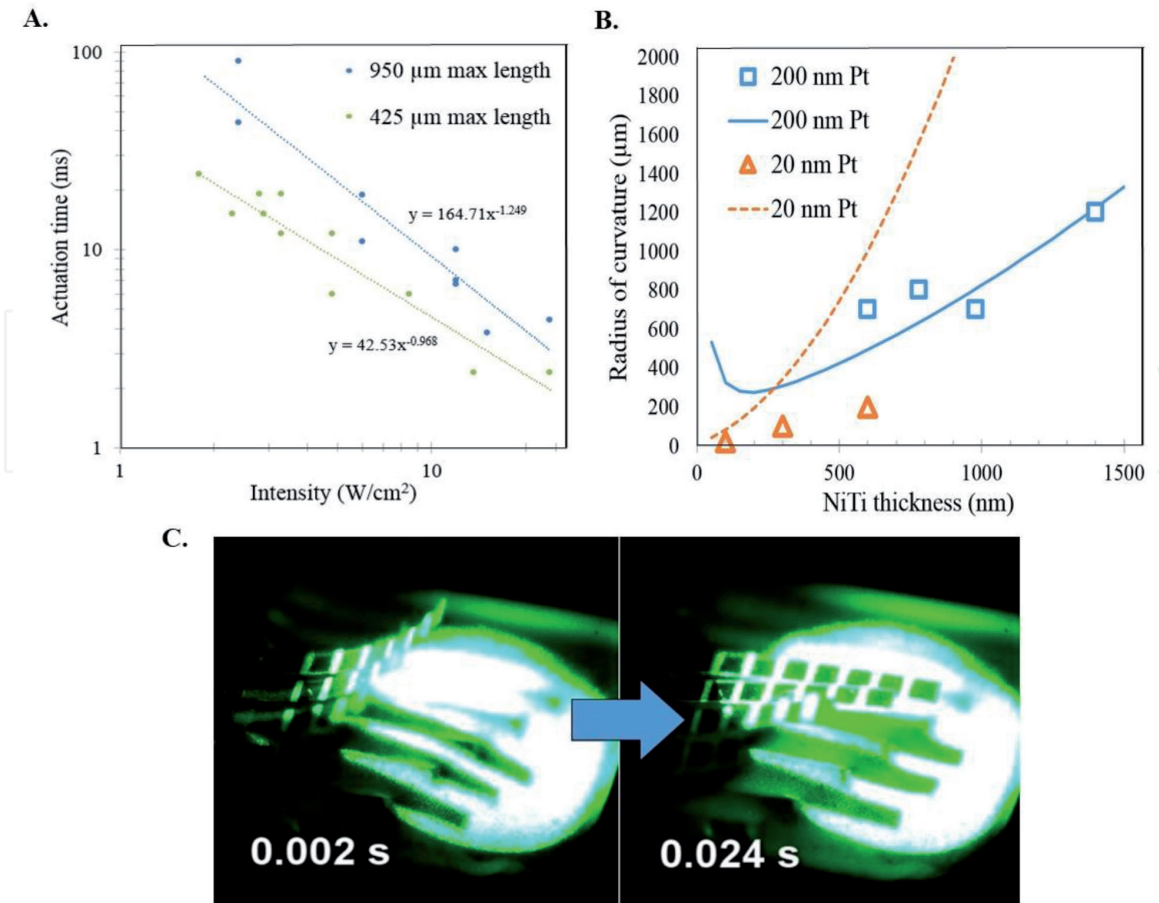
Figure 2.
(A) Actuation time vs. laser irradiance for 600 nm NiTi on 20 nm Pt bimorphs, (B) calculated and measured curvature radius for thermally activated NiTi on Pt bimorphs (1.4 μm on 200 nm Pt), and (C) demonstration of passive laser irradiated device-specific actuation with a 532 nm "green" laser (~7.2 W/cm²) in 24 ms for the 1.4 μm thick NiTi device stack.

density as shown in **Figure 2A**. As would be expected for a cantilever beam clamped on one end to a heat sink, the actuation time followed a $1/I2$ (I, being intensity) power law. Overall, the devices could be fully actuated in under 20 ms with intensities as low as 2 W/cm^2. The response time decreased to 3 ms with intensities over 14 W/cm^2. As shown in **Figure 2C**, 1.4 μm thick NiTi on 200 nm Pt devices actuated into their downward state within 25 ms when irradiated at 7.2 W/cm^2. A slower actuation time of 230 ms was observed at 1.44 W/cm^2. The radius of curvature for the 600 nm NiTi/20 nm Pt stack was 5.4X tighter (200 μm), compared to the 1.2 mm curvature in the 1.4 μm thick NiTi stack. For the tightest curling (200 μm) 600 nm thick NiTi devices, we performed a dynamic optical actuation experiment where we measured actuation time at various laser intensities. These results are plotted in **Figure 2A**.

3.3 Electrical actuation (joule heating) SMA MEMS

Figure 3A shows schematic of the joule heated SEM MEMS resistor actuator including cross section. The bond pads for electrical probe pads or wire bonding are comprised on 200 micron squares of NiTi alloy. The cross section is comprised of 1 micron thick SU-8 epoxy on top of the 270 nm thick NiTi, with reversible SMA properties. We fabricated joule heaters with various widths and lengths (10, 15, 20) and (100, 150, 200, 300, and 400) microns, respectively. The large CTE mismatch between SU-8 and NiTi drives the upward curvature of

the MEMS actuator post-release. **Figure 3B** shows SEM of the released actuator. **Figure 3C** depicts the fabrication process flow used to build the actuator, whereby NiTi is patterned with ion milling, and the release etch is done in XeF_2. **Figure 3D** shows the thermal actuation of the actuator which is characterized by large, non-linear changes in deflection upon subsequent heating and cooling cycles.
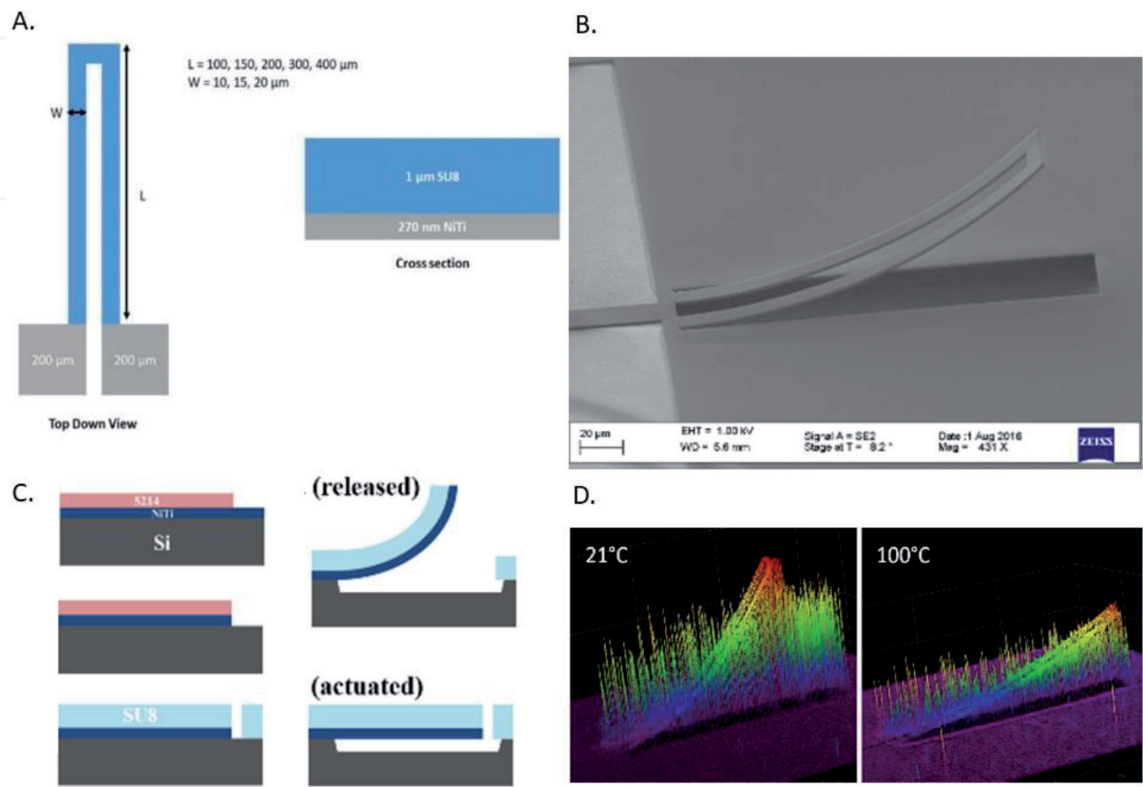

Figure 3.
(A) Schematic of the joule heated SEM MEMS resistor actuator including cross section, (B) SEM of released actuator, (C) fabrication process flow used to build the actuator, and (D) thermal actuation of the actuator.
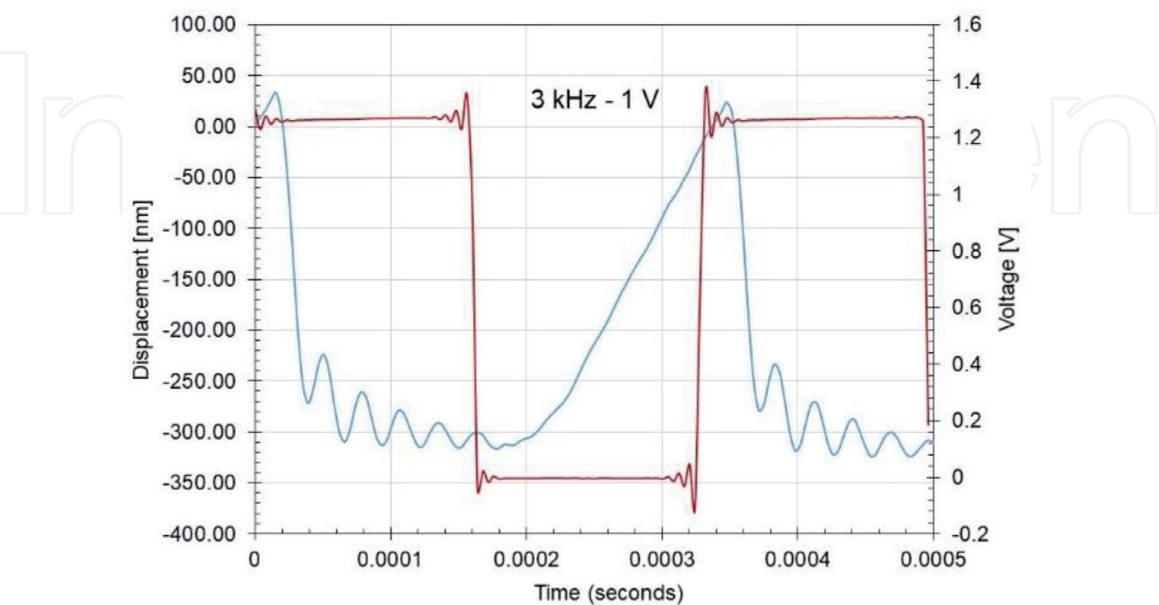

Figure 4.
Measured displacement of SMA MEMS resistively heated actuator vs. time for a 1 V pulsed square wave (50% duty cycle) at 3 kHz.

Figure 4 shows the measured deflection of the actuator using a 1 V pulsed current with 50% duty cycle at 3 kHz. For these devices the total power drawn was measured to be 5–15 mW.

4. Conclusion

In conclusion, we were able to demonstrate novel applications of the SMA MEMS actuator including both low power laser and low power and fast electrical joule heating. In other words, the SMA can be actuated by absorbing laser energy in the form of heat, or through pulsed electrical current. This was enabled by the development of deposition and characterizations of nanoscale thickness NiTi thin films. NiTi thin films with reversible changes in recovery stress were mated with other residual stressed thin films to enable reversible thermal actuation at MEMS scale. By incorporating nanoscale thin film SMA MEMS with good heat sinking design, we could achieve reversible actuations up to 3 kHz which is significantly greater than many previous reports for SMA actuators.

Acknowledgements

Conflict of interest

No conflict of interests.

Notes/Thanks/Other declarations

Place any other declarations, such as "Notes", "Thanks", etc. in before the References section. Assign the appropriate heading.

Author details

Cory R. Knick
US Army Research Laboratory (ARL), US Army Night Vision and Electronic
Sensors Directorate, Ft. Belvoir, VA, USA

*Address all correspondence to: cory.r.knick.civ@mail.mil

IntechOpen

References

[1] Busch JD, Johnson AD, Lee CH, Stevenson DA. Shape-memory properties in Ni-Ti sputter-deposited film. Journal of Applied Physics. 1990;**68**(12):6224-6228. DOI: 10.1063/1.346914

[2] Chen-Luen Shih B-KL, Kahn H, Phillips SM, Heuer AH. A robust co-sputtering fabrication procedure for TiNi shape memory alloys for MEMS. JMEMS. 2001;**10**:69-79

[3] Otsuka K, Ren X. Physical metallurgy of Ti–Ni-based shape memory alloys. Progress in Materials Science. 2005;**50**(5):511-678. DOI: 10.1016/j.pmatsci.2004.10.001

[4] Choudhary N, Kaur D. Shape memory alloy thin films and heterostructures for MEMS applications: A review. Sensors and Actuators A: Physical. 2016;**242**:162-181. DOI: 10.1016/j.sna.2016.02.026

[5] Cory R Knick DJS, Wilson AA, Smith GL, Morris CJ, Bruck HA. High frequency, low power, electrically actuated shape memory alloy MEMS bimorph thermal actuators. Journal of Micromechanics and Microengineering. 2019;**29**(7):23

[6] Dahmardeh M et al. High-power MEMS switch enabled by carbon-nanotube contact and shape-memory-alloy actuator. Physica Status Solidi A. 2013;**210**(4):631-638. DOI: 10.1002/pssa.201228678

[7] Lambrecht IAF, Chernenko V, Kohl M. Integrated SMA-based NEMS actuator for optical switching. In: IEEE 29th International Conference on Micro Electro Mechanical Systems (MEMS); Shanghai, China; 2016. pp. 79-82. DOI: 10.1109/MEMSYS.2016.7421562

[8] Wolf RH, Heuer AH. TiNi (shape memory) films on Si for MEMS applications. Journal of Microelectromechanical Systems. 1995;**4**:4

[9] Knick CR, Smith GL, Morris CJ, Bruck HA. Rapid and low power laser actuation of sputter-deposited NiTi shape memory alloy (SMA) MEMS thermal bimorph actuators. Sensors and Actuators A: Physical. 2019;**291**:48-57. DOI: 10.1016/j.sna.2019.03.016

[10] Mohamed Ali MS, Bycraft B, Bsoul A, Takahata K. Radio-controlled microactuator based on shape-memory-alloy spiral-coil inductor. Journal of Microelectromechanical Systems. 2013;**22**(2):331-338. DOI: 10.1109/jmems.2012.2221161

[11] Namazu T, Tashiro Y, Inoue S. Ti–Ni shape memory alloy film-actuated microstructures for a MEMS probe card. Journal of Micromechanics and Microengineering. 2007;**17**(1):154-162. DOI: 10.1088/0960-1317/17/1/020

[12] Wibowo E et al. Two-way actuation of bilayer cantilever of nickel titanium and silicon nitride thin films by shape memory effect and stress relaxation. In: Presented at The Device and Process Technologies for MEMS, Microelectronics, and Photonics III; 2004

[13] Isalgue VTA, Seguin JL, Bendahan M, Esteve-Cano. Shape memory NiTi thin films deposited at low temperature. Materials Science and Engineering A. 1999;**273-275**:717-721

[14] Bechtold C, Chluba C, Lima de Miranda R, Quandt E. High cyclic stability of the elastocaloric effect in sputtered TiNiCu shape memory films. Applied Physics Letters. 2012;**101**(9):091903. DOI: 10.1063/1.4748307

[15] Fu YQ et al. On the lower thickness boundary of sputtered TiNi films

for shape memory application. Thin Solid Films. 2006;**515**(1):80-86. DOI: 10.1016/j.tsf.2005.12.039

[16] Huang X, Liu Y. Surface morphology of sputtered NiTi-based shape memory alloy thin films. Surface and Coatings Technology. 2005;**190**(2-3):400-405. DOI: 10.1016/j.surfcoat.2004.02.029

[17] Inoue S, Morino K, Yoshiki K, Namazu T. Effect of substrate temperature on the shape memory behavior of Ti-Ni-Cu ternary alloy sputtered films. Materials Science Forum. 2012;**706-709**:1903-1908. DOI: 10.4028/www.scientific.net/MSF.706-709.1903

[18] Martins RMS, Schell N, Mahesh KK, Pereira L, Silva RJC, Braz Fernandes FM. Texture development and phase transformation behavior of sputtered Ni-Ti films. Journal of Materials Engineering and Performance. 2009;**18**(5-6):543-547. DOI: 10.1007/s11665-009-9484-9

[19] Martins RMS et al. Texture development, microstructure and phase transformation characteristics of sputtered Ni–Ti shape memory alloy films grown on TiN<111>. Thin Solid Films. 2010;**519**(1):122-128. DOI: 10.1016/j.tsf.2010.07.078

[20] Wibowo E, Kwok CY. Fabrication and characterization of sputtered NiTi shape memory thin films. Journal of Micromechanics and Microengineering. 2006;**16**(1):101-108. DOI: 10.1088/0960-1317/16/1/014

[21] Satoh G, Birnbaum A, Yao YL. Annealing effect on the shape memory properties of amorphous NiTi thin films. Journal of Manufacturing Science and Engineering. 2010;**132**(5):051004-1-051004-9. DOI: 10.1115/1.4002189

[22] Lee H-J, Ramirez AG. Crystallization and phase transformations in amorphous NiTi thin films for microelectromechanical systems. Applied Physics Letters. 2004;**85**(7):1146-1148. DOI: 10.1063/1.1783011

[23] Gisser KRC, Busch JD, Johnson AD, Ellis AB. Oriented nickel-titanium shape memory alloy films prepared by annealing during deposition. Applied Physics Letters. 1992;**61**(14):1632-1634. DOI: 10.1063/1.108434

[24] Kenneth Ainslie CK, Smith G, Li J, Troxel C, Mehta A, Kukreja R. Controlling shape memory effects in NiTi thin films grown on Ru seed layer. Sensors and Actuators A: Physical. 2019;**294**:7. DOI: 10.1016/j.sna.2019.04.047

[25] Ishida A, Sato M. Development of polyimide/SMA thin-film actuator. Materials Science Forum. 2010;**654-656**:2075-2078. DOI: 10.4028/www.scientific.net/MSF.654-656.2075

[26] Ishida A, Sato M. Ti–Ni–Cu shape-memory alloy thin film formed on polyimide substrate. Thin Solid Films. 2008;**516**(21):7836-7839. DOI: 10.1016/j.tsf.2008.04.091

[27] Kishi Y, Ikenaga N, Sakudo N, Yajima Z. Shape memory behavior of TiNi alloy films sputter-deposited on polyimide substrate. Journal of Alloys and Compounds. 2013;**577**:S210-S214. DOI: 10.1016/j.jallcom.2012.02.020

[28] Kotnur VG, Tichelaar FD, Fu WT, De Hosson JTM, Janssen GCAM. Shape memory NiTi thin films deposited on polyimide at low temperature. Surface and Coatings Technology. 2014;**258**:1145-1151. DOI: 10.1016/j.surfcoat.2014.07.018

[29] Kabla M, Seiner H, Musilova M, Landa M, Shilo D. The relationships between sputter deposition conditions, grain size, and phase transformation temperatures in NiTi thin films.

Acta Materialia. 2014;**70**:79-91. DOI: 10.1016/j.actamat.2014.02.009

[30] Kumar A, Singh D, Kaur D. Grain size effect on structural, electrical and mechanical properties of NiTi thin films deposited by magnetron co-sputtering. Surface and Coatings Technology. 2009;**203**(12):1596-1603. DOI: 10.1016/j.surfcoat.2008.12.005

[31] Pan G, Cao Z, Wei M, Shi J, Xu L, Meng X. Thickness and grain size dependence of B2–R martensitic transformation behaviors in nanoscale TiNi films. Materials Letters. 2014;**130**:285-288. DOI: 10.1016/j.matlet.2014.05.129

[32] Ryklina EP, Polyakova KA, Tabachkova NY, Resnina NN, Prokoshkin SD. Effect of B2 austenite grain size and aging time on microstructure and transformation behavior of thermomechanically treated titanium nickelide. Journal of Alloys and Compounds. 2018;**764**:626-638. DOI: 10.1016/j.jallcom.2018.06.102

[33] Shi XB, Guo FM, Zhang JS, Ding HL, Cui LS. Grain size effect on stress hysteresis of nanocrystalline NiTi alloys. Journal of Alloys and Compounds. 2016;**688**:62-68. DOI: 10.1016/j.jallcom.2016.07.168

[34] Shu YC, Bhattacharya K. The influence of texture on the shape memory effect in polycrystals. Acta Metallurgica. 1998;**46**(15)

[35] Shin DD, Mohanchandra KP, Carman GP. High frequency actuation of thin film NiTi. Sensors and Actuators A: Physical. 2004;**111**(2-3):166-171. DOI: 10.1016/j.sna.2003.09.026

[36] Velez C, Patel D, Kim S, Babaei M, Knick C, Smith G, et al. Combining micro fabrication and additive manufacturing for microrobotic mechanisms. In: Special Proceedings of JMEMS Combining Micro Fabrication and Additive Manufacturing for Microrobotic Mechanisms; 2020

[37] Camilo Velez SK, Patel D, Babaei M, Knick CR, Smith G, Bergbreiter S. Rapid prototyping of microactuators by integrating 3D printed polymeric structures with NiTi thin film. In: Presented at the 33rd IEEE International Conference on Micro Electromechanical Systems (MEMS); 2020

[38] Hyun-Taek Lee MSK, Lee G-Y, Kim C-S, Ahn S-H. Shape memory alloy (SMA)-based microscale actuators with 60% deformation rate and 1.6 kHz actuation speed. Small. 2018;**14**(3)

[39] Rastjoo S, Fechner R, Bumke L, Kötz M, Quandt E, Kohl M. Development and co-integration of a SMA/Si bimorph nanoactuator for Si photonic circuits. Microelectronic Engineering. 2020;**225**:111257-11262. DOI: 10.1016/j.mee.2020.111257